SAND2007-8170C

# Skeletal mechanism generation with CSP and validation for premixed n-heptane flames

Jens Prager [a], Habib N. Najm [a], Mauro Valorani [b], Dimitris A. Goussis [c]

[a] *Sandia National Laboratories, Livermore, CA 94550, USA*
[b] *Universita di Roma "La Sapienza", Rome, Italy*
[c] *National Technical University of Athens, Ploutonos 7, Athens, Greece*

**Abstract**

The Computational Singular Perturbation (CSP) method has been used to generate skeletal reaction mechanisms for the combustion of n-heptane/air mixtures at equivalence ratios between 0.5 and 2.0 and different pressures. The method uses a database of importance indices that were obtained from homogeneous n-heptane/air ignition computations. In this paper we examine the accuracy of these simplified mechanisms when they are used for laminar n-heptane/air premixed flames. The objective is to evaluate the accuracy of these simplified models when transport processes lead to local mixture compositions that are not necessarily part of the comprehensive homogeneous ignition databases. The detailed mechanism was developed by Curran et al. and involves 560 species and 2538 reactions. The smallest skeletal mechanism considered consists of 66 species and 326 reactions. We show that these skeletal mechanisms yield good agreement with the detailed model for premixed n-heptane flames, over a wide range of equivalence ratios and pressures, for certain global/integral flame properties. On the other hand, while they exhibit good accuracy in predicting certain elements of internal flame structure, we find significantly large errors in the concentration of radical species, particularly in the region where low-temperature chemistry plays a role. We also observe that the low-temperature chemistry of n-heptane can play an important role at very lean or very rich mixtures, reaching these limits first at high pressure. This has implications on numerical simulations of non-premixed flames where these lean and rich regions occur naturally.

*Keywords:* Reduced chemistry, Computational Singular Perturbation, n-heptane oxidation, premixed flame

## 1. Introduction

Numerical simulations of reactive flows using detailed chemistry are extremely demanding with respect to computational cost, especially if fuels are to be considered that are of high importance for a range of applications in automotive research, e.g. heptane, octane etc. The reaction mechanisms easily involve hundreds of species and thousands of reactions.

Several methods have been used to reduce the com-

putational cost associated with the chemical system. There are very good review articles about reduction methods, see for instance [1, 2]. Here, we will mention only recent efforts for the case of n-heptane oxidation.

The first main class of methods aims at replacing parts of the detailed model by global reaction steps whose rates are calculated based on the elementary reaction rates [3]. The generation of skeletal reaction mechanisms is the second main strategy to reduce the complexity of the chemical system. After the user specified a set of species that are to be modeled with high accuracy, the reduction method eliminates unimportant reactions [4] or eliminates unimportant species and reactions [5, 6].

We use Computational Singular Perturbation (CSP) to analyze the importance of reactions for the production and consumption of a set of target species and generate skeletal mechanisms by removing unimportant species. In previous publications we demonstrated that this strategy leads to mechanisms that can be used to accurately model the ignition of n-heptane/air mixtures at constant pressure and constant volume [7, 8]. The simplification strategy in these studies relies on a computed database of mixture compositions, temperature, and pressure, developed using homogeneous ignition computations over ranges of initial conditions. Therefore, the accuracy of these mechanisms is not examined outside of the range of mixture conditions visited in the ignition computations. The question then, is whether transport processes in premixed flames, over similar ranges of reactant conditions, lead to internal local mixture conditions that fall sufficiently outside the ignition databases to lead to large errors when using these mechanisms. This is the issue addressed in the present study. Specifically, we investigate the utility of these skeletal mechanisms for computations of laminar premixed flames of n-heptane/air mixtures at different equivalence ratios and pressures. We evaluate the overall performance of the simplified mechanisms in computed global/integral flame properties and dominant species profiles. We also evaluate the accuracy of prediction of radical species in different regions of the flame structure. We pay particular attention to the low-temperature region of the flame where many of the important reactions were removed in the simplification process. This is done over ranges of equivalence ratio and pressure. We also comment on the observed time scale structure in the flame using detailed versus simplified mechanisms, based on CSP analysis of the computed flame results. We use these observations, along with CPU timing studies, to evaluate computational gains afforded by the simplified models.

## 2. Methods

The reduction method has been presented already in detail elsewhere [7, 8]. Therefore, we only want to repeat the main ideas here. As the starting point we use the detailed mechanism of Curran et al. [9–11]. This mechanism consists of 560 species and 2538 reactions. It is comprehensive over a wide range of equivalence ratios and pressures. It includes the low-temperature and the high-temperature chemistry of n-heptane oxidation.

### *2.1. Mechanism reduction*

The reduction strategy is based on the separation of fast and slow chemical processes offered by the CSP method [12]. It has the advantage of being highly automated with minimal required input and a high confidence in the resulting skeletal mechanisms.

The simplification algorithm consists of three main stages. First, at each computed state of the chemical system, a set of locally important species is identified iteratively. This done by starting from the user-defined set of target species and adding all species to the set of target species that are involved in reactions with them and which corresponding reactions have a CSP-importance index larger than a pre-defined threshold. Both the slow and the fast subspaces are considered. As the second step, all local sets of target species are combined to a comprehensive set of species. Finally, the skeletal mechanism is compiled from all reactions that only involve target species.

In this paper we study two different sets of skeletal mechanisms. The first set was constructed from homogeneous ignition calculations at a constant pressure of 1 atm. The CSP importance indices were determined for equivalence ratios $\phi$=0.5/1.0/2.0 and inital temperatures of 600/700/1000/1250 K. We chose a mechanism with 139 species and 612 reactions that showed very good agreement with the detailed model in these ignition calculations [7]. It is expected that the low-temperature chemistry of n-heptane is of minor importance in premixed laminar flames. In order to test this assumption, one skeletal mechanism is compiled from CSP importance indices at high temperatures only (1000 and 1250 K). This mechanism contains only 66 species and 326 reactions. In the following we refer to these mechanism as M139 and M66.

The second set of skeletal mechanisms is comprehensive over a pressure range for a fixed equivalence ratio of 1.0. It is constructed from calculations of homogenous ignition at constant volume for a stoichiometric mixture at initial pressures between 6.5 and 40 bar and a range of initial temperatures of 640 to 1240 K. Here, we consider two mechanisms (177 and 124 species) that result from different error tolerances in the reduction method. The larger mechanism reproduced the ignition delay times over the whole range of pressures and temperatures very well, while the second one results in shorter ignition delay times (up to a factor of 3) in the NTC region between approximately 800 and 1000 K [8]. M177 consists of 768 reactions, M124 has 525 reactions.

The skeletal mechanisms can be found in the supplement S1 (M177), S2 (M139), S3 (M124), S4

(M66) or from the authors.

### 2.2. Flame calculations

The PREMIX [13] tool of CHEMKIN-II is used for the flame computations. The species profiles which result from the different reduced mechanisms are locked spatially to each other by requiring that the flame temperature reaches 500 K at 0.8 cm in the 1 atm case, and at 0.05 cm for the 25/50 atm cases.

We use a $2^{nd}$-order reacting flow solver [14, 15] to compute chemical source terms needed to examine internal flame structure, reaction flow analysis, and CSP importance indices. This code solves the time-dependent reacting flow equations in the low-Mach number limit. It uses a mixture-averaged transport model [16], whose database we extended to include the species in the present detailed n-heptane mechanism. We used the PREMIX results as an initial condition for the time-dependent solver. This process involves interpolation of the solution between the meshes of the two solvers, with associated truncation errors. These errors, while small, do excite fast chemical processes in the flame. We relaxed the the solution over a sufficient time interval (500 ns) for these fast processes to relax.

## 3. Results

Considering that the simplified mechanisms were constructed sampling CSP importance indices from homogeneous ignition calculations at a restricted number of conditions – i.e. mixture composition, initial temperature, and pressure – testing the skeletal mechanisms on premixed laminar flames aims to examine the extent to which these two different chemical systems span a similar phase space.

The first set of reduced mechanisms (M139 and M66) was developed for use at atmospheric pressure and the range of stoichiometries between $\phi$=0.5 to 2.0 [8], using constant-pressure ignition computations. The second set (M177 and M124) was developed for a fixed stoichiometry of $\phi$=1.0, using constant-volume ignition computations, over the range of initial pressures between 6.5 and 40 bar [7].

### 3.1. Temperature profiles

Figure 1 shows the temperature profiles along the flame for different stoichiometries at 1 atm, for the first set of mechanisms. The temperature profiles agree well, with slightly larger errors between the simplified and detailed mechanisms in the lean and rich cases. The second set of mechanisms shows also good agreement in the temperature profiles when the pressure is varied from 1 to 50 atm, Fig. 2. Note that, for visual comparison convenience, we scaled the spatial coordinate in this figure by multiplying it with the pressure used, and shifted the profiles so that they coincide at 500 K. The smallest mechanism M124 leads generally to a slower rise in temperature, best seen in the two flames at higher pressure. The agreement is best for the flame at atmospheric pressure.

Note that we find superadiabatic flame temperatures in the fuel-rich cases at 1 and 50 atm as observed elsewhere for methane, acetylene, ethylene, and propane flames [17, 18]. Even though the maximum temperature differs between the 1 and 50 atm cases, the relative increase compared to the equilibrium temperature is almost the same in both cases, namely 1.2% and 1.6%.

### 3.2. Flame velocity

Tables 1 and 2 compare the adiabatic flame velocities that result from the two sets of mechanisms at different stoichiometries at 1 atm and at different pressures for $\phi$=1.0.

Overall, the flame velocities are well reproduced by the skeletal mechanisms, even by M66 in its range of validity ($\phi$=0.5-2.0). M139 has larger errors in the rich case. M66 shows larger errors on the lean side. When the stoichiometry range for which it was constructed is slightly exceeded to the lean side ($\phi$=0.4) these errors become somewhat larger. M66 yields a 7% lower flame velocity in this case (4.53 cm/s instead of 4.87 cm/s) while M139 reproduces the flame velocity exactly. The second set of mechanisms does not show a strong dependence of the errors on the pressure. The most reduced mechanism M124 yields lower flame velocities in all cases.

### 3.3. Species profiles

To measure the error $e_i$ in species mole-fraction profiles along the flame we determine their maximum deviation with respect to the results of the detailed mechanism and divide by the maximum value of the species mole fraction:

$$e_i^{red} = \frac{\max_x(|X_i^{det} - X_i^{red}|)}{\max_x(X_i^{det})} \quad . \qquad (1)$$

Here, $X_i$ denotes the mole fraction of species $i$, with the superscript indicating the use of the detailed ("$det$") or reduced mechanism ("$red$"). This error measure clearly leads to increased errors if the species profiles are simply shifted with respect to each other. We will discuss this issue further below.

The temperature and the concentrations of n-heptane and $CO_2$ were chosen as important observables in the construction of the mechanisms, so they should be well represented by the skeletal mechanisms. The accuracy of other species cannot be guaranteed by the method [19] unless they are included in the list of important observables. The mole fractions of n-heptane, $CO_2$, and other main species ($O_2$, $H_2O$, $H_2$, CO) are very well reproduced by the two skeletal mechanisms at 1 atm, see Tab. 3. The errors are well below 10%.

The errors increase in the majority of the cases when M66 is used, as may be expected. But, due

to the non-continuous nature of the reduction strategy, a smooth reduction of errors with the number of species retained in the mechanism cannot be guaranteed. There are some species, e.g. CO at $\phi$=1.0 in Tab. 3, that are better reproduced by the M66 mechanism than by M139.

The results for some major species from the second set of mechanisms are shown in Tab. 4. The errors reach up to 5% for M177 and 13% for M124. The errors are smallest for 1 atm, while the errors at 25 atm and 50 atm are comparable. M177 performs clearly better in all the cases.

Even though the accuracy of the species not included in the list of important species is not strictly guaranteed by the reduction method, it is instructive to examine the impact of these different degrees of simplification on the prediction of other species in the flame. Thus, in the following we examine internal flame structure as computed by the different mechanisms.

Considering errors in *all* species, we find that, within the first set of mechanisms, M139 performs best in the stoichiometric case. In this case, half of the species exhibit errors less than $\sim$ 20%. In fact, we find only about 10 species with errors larger than 100%. These are pentyl and heptyl hydroperoxy radicals and their ketohydroperoxides. The largest errors observed (factor of 20) are for $C_7H_{14}OOH_{1-4}$. These species are active in the low-temperature chemistry of n-heptane.

In the fuel-lean and rich cases the errors increase, so that half of the species deviate by up to $\sim$ 60%. The rich flame shows larger errors compared to the lean flame. There, we find a bimodal distribution of errors, one centered around errors of 20%, and the other around 2000%. In general, we find that the largest errors occur in species related to the low-temperature chemistry in the region of the flame with temperatures below 1000 K. But we also find larger errors in major species in the rich flame – e.g. n-heptane itself with 10% – see Tab. 3.

M66 also shows the smallest errors in the stoichiometric case, but in contrast to M139, the rich flame is better reproduced. Half the species have errors less than $\sim$ 30%. The error distribution does not show the bimodal features found in the 139-species mechanism. Overall, the fraction of species with errors in excess of 100% is decreased with respect to the 139-species mechanism. This is the result of the elimination of species participating in the low-temperature chemistry in M66. Species with the largest errors are now: $C_3H_5O$, $C_2H_5O$, $C_2H_5CHO$, $C_4H_7$. The errors are smallest for the rich flame, ranging from 30% to 100%. In the lean case the deviations are around 100% with the exception of $C_2H_5CHO$ for which we find an error of 500%.

In the second set of mechanisms, M177 exhibits errors of less than 30% for half the species, with relatively little dependence on pressure. $C_4H_7$, $C_3H_5$, and some low-temperature species have the largest errors, up to 140%. M124 yields the best results for atmospheric pressure. Half the species have errors less than 30%. At both higher pressures, half the species have errors up to 60%. Species with the largest errors are $C_4H_7$, $CH_2CHO$, $C_3H_4$, and several low-temperature species for which error levels reach up to 3000%.

We also computed the stoichiometric flame at 50 atm with the smallest mechanism M66. Even though this mechanism has been produced from ignition data at 1 atm only it produces results comparable to the two mechanisms that are comprehensive over pressure. The errors calculated by Eq. (1) are even smaller compared to M124 (mean error 13% versus 26%). The flame velocity is 21.3 cm/s, the same as that obtained by the detailed mechanism.

If we compare the maxima of the species profiles instead of the maximumum deviation, i.e. by using

$$e_i^{red} = \frac{|\max_x(X_i^{det}) - \max_x(X_i^{red})|}{\max_x(X_i^{det})} \quad , \qquad (2)$$

we generally find smaller errors for most of the species. This shows that some species profiles are shifted to some extent. These shifts result from the slightly different temperature profiles between the detailed and simplified models. If we use Eq. 2 for the results of the second set of mechanisms, we find that the deviations by M177 do not depend strongly on the error measure. Half the species still have errors below 30%. There is a reduced error for the flame at 50 atm, now half the species show errors less than 20%. The influence of the error measure is much larger for M124. At all three pressures we find overall a reduced error, the effect being largest for the flame at 50 atm. Instead of 60%, half the species show errors of less than 30%. The overall errors of the first set of mechanisms depends only slightly on the way the error is calculated. This is consistent with the deviations in the temperature profiles that we observed.

If we compare the errors calculated by Eq. (2) M124 and M66 have roughly the same average accuracy.

### *3.4. Heat release rate*

Figure 3 shows profiles of the heat-release rate for different stoichiometries at 1 atm. We find good agreement for all cases within the range of stoichiometries for which the mechanisms were developed (0.5 to 2.0), with the maximum heat-release rate reproduced to within 4%. In the second set of mechanisms (not shown), M177 reproduces the maximum heat-release rate well, the errors are less than 2%. M124 always yields rates that are smaller by about 10-12%.

It is interesting to note that there is a region with net endothermic behaviour in the rich flame at atmospheric pressure, on the reactants side of the primary flame heat release rate peak. Analysis of the results indicates that this is largely due to thermal decomposition reactions of the several alkyl radicals, e.g.

$C_2H_5$, n-$C_3H_7$, $C_4H_9$, $C_5H_{11}$, $C_7H_{15}$, and n-heptane itself.

If we leave the original range of stoichiometries (e.g. for $\phi$=0.4) we find significantly larger differences. All the heat-release profiles (M560) show – a more or less pronounced – first peak in the low-temperature region before the main heat release. This peak becomes comparable to the main peak of heat release in the very lean and rich flames. The total heat release rate is much smaller in these cases, and the low-temperature zone of the flame is enlarged. Because the low-temperature chemistry was removed in M66, this mechanism can be used to examine situations in which this chemistry plays an important role. The absence of low-temperature chemistry in this mechanism is evident in its missing heat-release peak ($\phi$=0.4) in Fig. 3. These differences seen at $\phi$=0.4 still lead to only small deviations in the predicted temperature profiles, as shown in Fig. 1. We also find an increased importance of the low-temperature regime under rich conditions ($\phi$=2.5/1 atm), see the temperature and heat-release rate profiles in Fig. 4. Here we find a significantly steeper temperature rise caused by the first peak of heat release. Significant deviations can also be found for important radicals in this region, e.g. H, OH, HCO, $HO_2$, and $H_2O_2$. The latter two reach significant concentrations in this low-temperature region; $H_2O_2$ has its maximum there and $HO_2$ a significant local maximum, see Fig. 5.

CSP can be used to analyze which reactions and transport processes determine the temperature evolution along the flame. We do this analysis for the detailed mechanism M560 and for M139 at the position in the flame of the low-temperature maximum of the heat-release rate ($\phi$=0.4 and 2.5 at 1 atm).

The analysis of the CSP importance indices for each reaction with respect to temperature at the first peak of heat release shows the importance of similar reactions in the lean and rich case:

$$\begin{aligned} \mathrm{n-C_7H_{16}+OH} &= \mathrm{C_7H_{15}+H_2O} \\ \mathrm{C_7H_{15}+O_2} &= \mathrm{C_7H_{15}O_2} \\ \mathrm{n-C_3H_7+O_2} &= \mathrm{n-C_3H_7O_2} \\ \mathrm{C_2H_5+O_2} &= \mathrm{C_2H_5O_2} \\ \mathrm{CH_3+O_2+M} &= \mathrm{CH_3O_2+M} \quad . \end{aligned}$$

These reactions – except for the radical attack of n-heptane – are oxygen addition reactions of heptyl radicals, which are the first reactions of the regular pathway of low-temperature chemistry.

### *3.5. Time scales and Computational effort*

It is interesting to see if the reduction method leads to a reduced stiffness of the chemical system by changing the smallest timescales. CSP provides information about the timescales in the flame and the participation indices can be used to determine which processes – reactions or transport – cause these timescales. The fastest timescale $\tau_1$ and the fastest timescale of the active modes $\tau_{M+1}$ are shown along the flame for different reduced mechanisms in Fig. 6. In addition, the temperature profile of the detailed model is plotted. This analysis is done for the stoichiometric flame at 1 atm.

We find very small timescales, on the order of $10^{-15}$ s, for M560 all along the flame. These fast timescales are related to reactions of the neopentane chemistry ("neoc5h9q2-n", "neoc5h10ooh-o2", "neoc5ket"). These reactions are eliminated by the reduction process in both mechanisms M139 and M66.

A timescale of $10^{-15}$ s is certainly an artifact of the reaction mechanism. The smallest average time between collisions of gas molecules in this flame is on the order of $10^{-10}$ s.

The smallest timescales of the M139 and M66 mechanisms are almost identical. In the cold region they are five orders of magnitude larger than for M560, in the hot region a factor of 20. Both show a minimum around 0.79 cm where the temperature is around 460 K and a peak at 0.8 cm at a temperature of 540 K. These peaks occur when another mode associated with the eigenvalues of the chemical system becomes the fastest one. On the left side of the marked region (see Fig. 6), diffusion of $H_2$ and $H_2O$ are the fastest processes. Within the marked region, the reactions

$$\begin{aligned} \mathrm{C_2H+H+M} &= \mathrm{C_2H_2+M} \\ \mathrm{C_3H_3+O} &= \mathrm{CH_2O+C_2H} \end{aligned}$$

become dominant in determining the fastest timescale. In the region with temperatures above 600 K (on the right of the marked region), the smallest timescales are caused by these reactions:

$$\begin{aligned} \mathrm{C_2H_3O_{1-2}} &= \mathrm{CH_3CO} \\ \mathrm{C_2H_3O_{1-2}} &= \mathrm{CH_2CHO} \quad . \end{aligned}$$

The smallest timescales of the active modes $\tau_{M+1}$ are comparable between the three mechanisms. In the reaction zone they reach their lowest values around $10^{-12}$ s.

Hence we find that the reduced mechanisms have a smaller range of timescales even though they are not constructed for this purpose. A further reduction of the skeletal mechanism does not necessarily lead to a further decrease of stiffness, as can be seen from M66 compared to M139.

To estimate the savings in computational time by the reduced mechanisms we measured the time per timestep during the propagation of the flames with our reactive-flow program. The results are shown in Tab. 5. The computation time scales approximately quadratically with the number of species and shows clearly the significance of skeletal mechanisms.

## 4. Conclusions

We presented calculations of laminar premixed flames using different skeletal mechanisms. The two

sets of mechanisms – one comprehensive over a range of stoichiometries at 1 atm, the other one over pressure for $\phi$=1.0 – showed good agreement with the detailed mechanism. The largest errors were found for species that participate in the low-temperature chemistry. Even though the mechanisms were developed from ignition calculations they yield good results in these inhomogeneous systems, also showing no strong dependence on pressure.

The lean and rich flames show an extended low-temperature zone, caused by the very low heat release rate at these conditions. In these cases it is important to include the low-temperature chemistry in reduced reaction mechanisms. Otherwise, the heat release rate and main radicals are not well predicted in the cold side of the flame. Extreme lean and rich conditions will occur naturally in non-premixed combustion, e.g. in edge flames. Larger errors have to be expected in this case if reduced mechanisms neglect the low-temperature chemistry.

## Acknowledgments

This work was supported by the US Department of Energy (DOE), Office of Basic Energy Sciences (BES), SciDAC Computational Chemistry Program; and by the DOE BES Division of Chemical Sciences, Geosciences, and Biosciences. Sandia National Laboratories is a multiprogram laboratory operated by Sandia Corporation, a Lockheed Martin Company, for the United States Department of Energy under contract DE-AC04-94-AL85000. MV acknowledges the support of the Italian Ministry of University and Research (MIUR).

## References

[1] M. Okino, M. Mavrovouniotis, *Chem. Rev.* 98 (1998) 391–408.

[2] A.S. Tomlin, T. Turányi, M.J. Pilling, *Comprehensive Chem. Kinet.* 35 (1997) 293–437.

[3] S.S. Ahmed, F. Mauss, G. Moréac, T. Zeuch, *Phys. Chem. Chem. Phys.* 9 (48) (2007) 1107–1126.

[4] B. Bhattacharjee, D.A. Schwer, P.I. Barton, W.H. Green Jr., *Combust. Flame* 135 (3) (2003) 191–208.

[5] T. Lu, C.K. Law, *Combust. Flame* 146 (3) (2006) 472–483.

[6] A. Saylam, M. Ribaucour, W.J. Pitz, R. Minetti, *Int. J. Chem. Kinet.* 39 (4) (2007) 181–196.

[7] M. Valorani, F. Creta, F. Donato, H.N. Najm, D.A. Goussis, in: P. Wesseling, E. Oñate, J. Périaux (Eds.), *ECCOMAS CFD 2006*, TU Delft, The Netherlands, 2006.

[8] M. Valorani, F. Creta, F. Donato, H.N. Najm, D.A. Goussis, *Proc. Combust. Inst.* 31 (2007) 483–490.

[9] H. Curran, P. Gaffuri, W. Pitz, C. Westbrook, available at http://www-cmls.llnl.gov/combustion/combustion2.html.

[10] H. Curran, P. Gaffuri, W. Pitz, C. Westbrook, *Combust. Flame* 129 (3) (2002) 253–280.

[11] H. Curran, P. Gaffuri, W. Pitz, C. Westbrook, *Combust. Flame* 114 (1-2) (1998) 149–177.

[12] S. Lam, D. Goussis, *Proc. Combust. Inst.* 22 (1988) 931–941.

[13] R.J. Kee, J.F. Grcar, M.D. Smooke, J.A. Miller, *A Fortran program for modeling steady laminar one-dimensional premixed flames*, Sandia Report SAND85-8240 UC-4, Sandia National Laboratories, 1985.

[14] O.M. Knio, H.N. Najm, and P.S. Wyckoff, *J. Comp. Phys.*, 154 (1999)

[15] H.N. Najm, O.M. Knio, *J. Sci. Comput.* 25 (1-2) (2005) 263–287. 428-467.

[16] P. Paul and J. Warnatz, *Twenty-Seventh Sympoium (Int.) on Combustion* (1998) 495-504.

[17] F. Liu, Ö.L. Gülder, *Combust. Flame* 143 (3) (2005) 264–281.

[18] V.V. Zamashchikov, I.G. Namyatov, V.A. Bunev, V.S. Babkin, *Combust. Explosions Shock Waves* 40 (1) (2004) 32–35.

[19] M. Valorani, F. Creta, D.A. Goussis, J.C. Lee, and H.N. Najm, *Combustion and Flame* 146 (2006) 29-51.

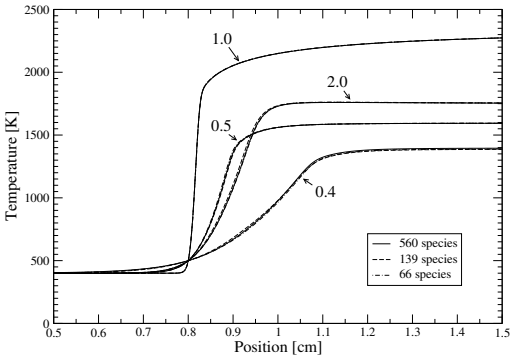


Fig. 1: Temperature profiles at 1 atm and different stoichiometries resulting from the three reaction mechanisms M560/M139/M66. The equivalence ratios used are indicated by the numbers next to the plots.

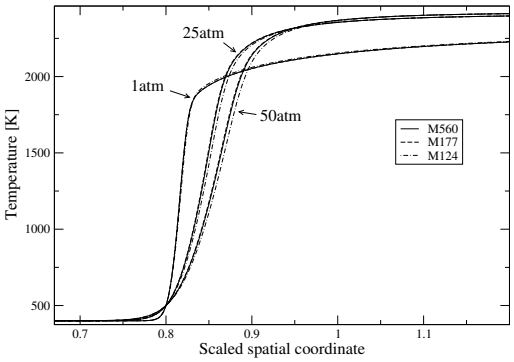


Fig. 2: Temperature profiles for $\phi$=1 at different pressures resulting from the mechanisms M560, M177, and M124. Pressures are indicated next to the plots. The spatial coordinate is scaled by the pressure. Thus, *e.g.* the units shown are in cm for the 1 atm case, and in 1/50 cm for the 50 atm case. The profiles are shifted to coincide at $T = 500$ K.

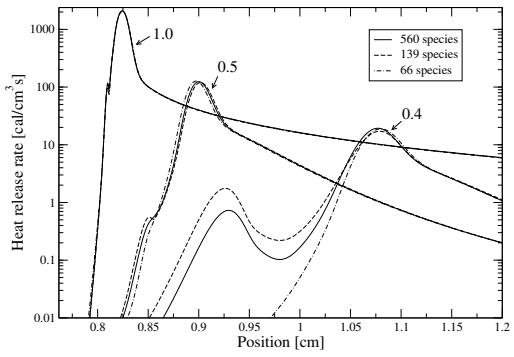


Fig. 3: Profiles of the heat release rate at 1 atm and different stoichiometries resulting from the three reaction mechanisms M560/M139/M66. The equivalence ratios used are indicteded by the numbers next to the plots.

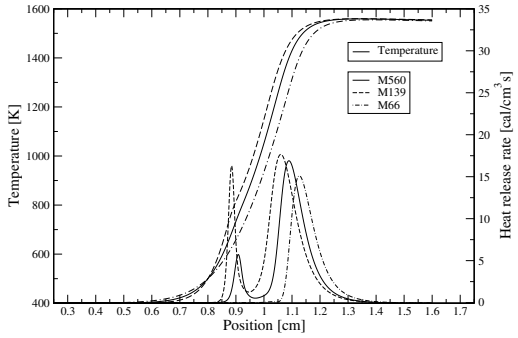


Fig. 4: Profiles of temperature and heat-release rate resulting from M560/M139/M66 for $\phi$=2.5 at 1 atm.

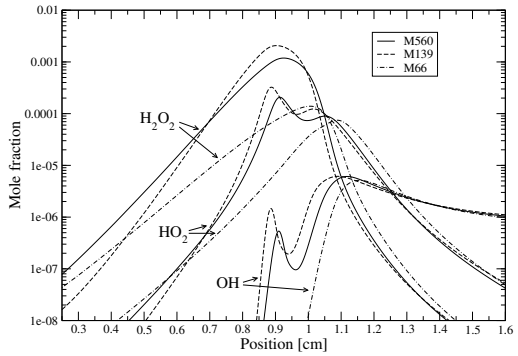


Fig. 5: Profiles of some radicals that participate in low-temperature chemistry resulting from M560/M139/M66 for $\phi$=2.5 at 1 atm.

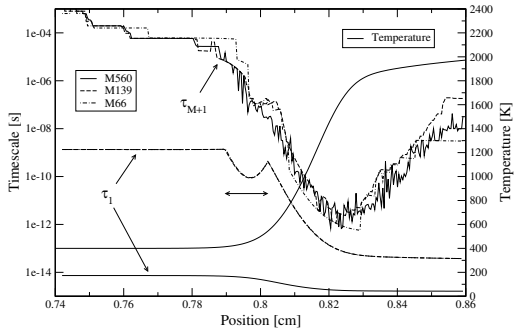


Fig. 6: Fastest timescales $\tau_1$ and fastest active timescale $\tau_{M+1}$ of the mechanisms M560/M139/M66 along the flame. In addition, the temperature profile of the detailed model is shown. Conditions are $\phi$=1 at 1 atm. The curves of $\tau_1$ for the reduced mechanisms M139 and M66 are undistinguishable.

| | $\phi$=0.5 | | $\phi$=1.0 | | $\phi$=2.0 | |
|---|---|---|---|---|---|---|
| M560 | 13.6 | – | 71.9 | – | 10.1 | – |
| M139 | 13.4 | -1.5% | 71.2 | -1.0% | 10.5 | +3.9% |
| M66 | 13.9 | +2.2% | 71.7 | -0.3% | 10.0 | -1.0% |

Table 1: Laminar flame velocities [cm/s] at 400 K/1 atm and different equivalence ratios $\phi$ resulting from the mechanisms M560, M139, M66. Percentages give the deviations with respect to M560.

| | 1 atm | | 25 atm | | 50 atm | |
|---|---|---|---|---|---|---|
| M560 | 71.9 | – | 27.8 | – | 21.3 | – |
| M177 | 72.5 | +0.8% | 28.2 | +1.4% | 21.6 | +1.4% |
| M124 | 68.6 | -4.6% | 26.2 | -5.8% | 20.2 | -5.2% |

Table 2: Laminar flame velocities [cm/s] at 400 K/$\phi$=1.0 and different pressures resulting from the mechanisms M560, M177, and M124. Percentages give the deviations with respect to M560.

| | $\phi$=0.5 | | $\phi$=1.0 | | $\phi$=2.0 | |
|---|---|---|---|---|---|---|
| | M139 | M66 | M139 | M66 | M139 | M66 |
| n-$C_7H_{16}$ | 1.8 | 4.0 | 0.4 | 1.5 | 10 | 3.3 |
| $O_2$ | 0.7 | 1.2 | 0.5 | 0.1 | 2.3 | 0.9 |
| $H_2O$ | 1.1 | 2.3 | 0.2 | 0.6 | 2.7 | 0.7 |
| CO | 2.9 | 4.3 | 1.2 | 0.4 | 2.9 | 1.9 |
| $CO_2$ | 1.5 | 2.2 | 0.4 | 0.1 | 0.9 | 1.8 |
| $H_2$ | 2.2 | 6.3 | 2.2 | 2.5 | 1.3 | 1.9 |

Table 3: Maximum errors of species profiles for major species in the premixed flames at 1 atm. Numbers are in percent calculated by Eq. (1).

| | 1atm | | 25atm | | 50atm | |
|---|---|---|---|---|---|---|
| | M177 | M124 | M177 | M124 | M177 | M124 |
| n-$C_7H_{16}$ | 2.9 | 6.0 | 5.0 | 9.7 | 4.5 | 9.1 |
| $O_2$ | 0.5 | 2.6 | 1.2 | 4.7 | 1.1 | 4.7 |
| $H_2O$ | 0.6 | 1.5 | 1.2 | 3.5 | 1.2 | 3.5 |
| CO | 0.9 | 7.3 | 2.2 | 10.8 | 2.0 | 10.5 |
| $CO_2$ | 0.2 | 1.2 | 0.8 | 4.1 | 0.8 | 4.3 |
| $H_2$ | 0.7 | 8.0 | 1.7 | 12.0 | 1.9 | 13.1 |

Table 4: Maximum errors of species profiles for major species in the premixed flames for $\phi$=1.0 at different pressures. Numbers are in percent calculated by Eq. (1).

| | M66 | M124 | M139 | M177 | M560 |
|---|---|---|---|---|---|
| time [s] | 13.1 | 38.8 | 49.4 | 79.3 | 1506 |

Table 5: Computation time per timestep using different reduced mechanisms. The time propagation has been done with 4096 grid points and a timestep of 1 ns, $\phi$=1.0 at 1 atm.